The American Journal of Human Genetics, Volume *103*

Supplemental Data

Squalene Synthase Deficiency: Clinical, Biochemical, and Molecular Characterization of a Defect in Cholesterol Biosynthesis

David Coman, Lisenka E.L.M. Vissers, Lisa G. Riley, Michael P. Kwint, Roxanna Hauck, Janet Koster, Sinje Geuer, Sarah Hopkins, Barbra Hallinan, Larry Sweetman, Udo F.H. Engelke, T. Andrew Burrow, John Cardinal, James McGill, Anita Inwood, Christine Gurnsey, Hans R. Waterham, John Christodoulou, Ron A. Wevers, and James Pitt

Supplemental Notes

Supplemental Case Reports

This research was approved by the Sydney Children's Hospitals Network Human Research Ethics Committee (HREC ID 10/CHW/114). Written informed consent was obtained from the parents of the affected individuals investigated in this study.

Individual 1 and 2:

These siblings are the product of non-consanguineous parents of European background. The salient features common to both include; intrauterine growth restriction (IUGR), facial dysmorphism, generalised seizures, hypoplastic corpus callosum, reduced age appropriate myelination, bilateral optic nerve hypoplasia with visual impairment, profound global developmental delay, irritability, post-natal failure to thrive, poor sleep initiation and maintenance, dry skin with photosensitivity, and gracile bones.

Urine organic acid profiles in both siblings consistently demonstrated an abnormal pattern of elevated mevalonate lactone, methylsuccinate and multiple branched-chain dicarboxylic acids which bore similarity to the patterns of animals treated with squalene synthase inhibitor drugs (5 samples in subject 1 and 4 samples in subject 4). Fasting cholesterol studies are summarized in Table 1, and consistently demonstrated low normal total cholesterol (TC) levels and reduced low-density lipoprotein cholesterol (LDL-C).

Individual 1

This female infant was delivered via a spontaneous vaginal delivery (SVD) at 37 weeks gestation after an uneventful pregnancy, with Apgar scores of 9 and 9 at one and five minutes respectively, a birth weight 2600g, head circumference 32.5cm, and length 47cm.

She developed generalised tonic-colonic seizures at five days of age, which were well controlled with phenobarbitone. Seizures have not been evident beyond the infantile period. An MRI of the brain at 9 months of age demonstrated a hypoplastic corpus callosum, and reduced white matter. Optic nerve hypoplasia was detected on fundoscopy and was associated with poor visual acuity. Anterior and posterior pituitary endocrine function were intact. Dysmorphic features included depressed nasal bridge, low set and posteriorly rotated ears, square nasal tip, epicanthic folds, mild micrognathia and mild retrognathia, and 2-3 toe syndactyly. Genitalia were normally formed.

Currently she is 10 years of age, and demonstrates profound global developmental delay in all modalities, in keeping with the milestone acquisition of a 6-month old child. She can roll and sit independently. She can manipulate objects to her mouth but is unable to feed herself. She is non-verbal, but does smile in response to verbal social interactions. Neurological examination demonstrates central hypotonia, hyperreflexia, and fixed flexion joint contractures at the knees. Irritability and autistic-like behaviors, such as habitual eye poking, have been evident since the first year of life. Hypersalivation has required medical interventions. Postnatal failure to thrive, compounded by an unsafe swallow, required the insertion of a PEG at 4 years of age for enteral feeding. Sleep initiation and maintenance are significant issues which have responded to melatonin supplementation. Dry skin and photosensitivity is evident with clinically significant UV sun damage after only 10 minutes in direct sunlight. A skeletal survey demonstrated thin gracile bones with reduced bone mineralization, but no skeletal axial fractures have been observed.

Individual 2

This male infant was delivered via a SVD at 39 weeks gestation after an uneventful pregnancy, with Apgar scores of 9 and 9 at one and five minutes respectively, a birth weight 2750g, head circumference 34cm, and length 49cm. His clinical course has mirrored that of his elder sister. He showed the same brain MRI changes, dysmorphic features, and bilateral undescended testes that required surgical intervention. He is currently 7 years of age, and demonstrates profound global developmental delay in all modalities, with an overall skill acquisition of a 9-month old child. He can sit independently, and pull to stand and will ambulate short distances on his knees. He can babble, smiles in response to verbal social interactions, but does not display meaningful social language.

Individual 3

This male infant was delivered at 39 weeks gestation after an uneventful pregnancy, with Apgar scores of 9 and 9 at one and five minutes respectively, a birth weight 3033grams, head circumference 33cm, and length 50cm. His clinical presentation in infancy was significant for severe static encephalopathy, intractable epilepsy, spasticity, opisthotonos, global developmental delay with cortical blindness, hypospadias, bicuspid aortic valve, neonatal hepatitis, dry skin, facial dysmorphism, failure to thrive and sleep dysfunction. Dysmorphism included coarse facial features, bitemporal narrowing, prominent ears, and triangular facies. MRI of the brain at 3 months of age demonstrated diffuse polymicrogyria involving the frontal, parietal, and temporal lobes with some central white matter and cortical volume loss. EEG demonstrated multifocal epileptiform discharges, but seizure control was high doses of levetiracetam, with only occasional breakthrough seizures during illnesses. He is

now 9 years of age and demonstrates severe global developmental delay, he attempts to sit and vocalizes without formation of clear words.

Supplemental Figures

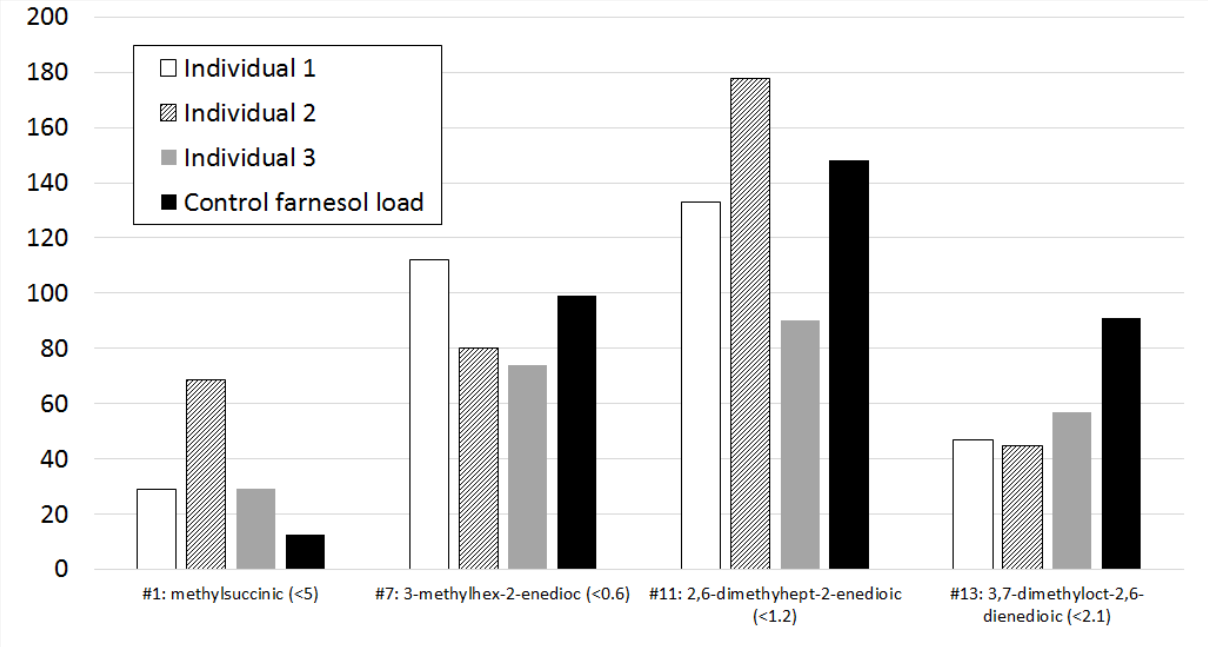

Figure S1: Urine metabolite concentrations in individuals and in a control after oral farnesol loading (urine collected 4.25 hours post load). Concentrations of the major dicarboxylic farnesol metabolites are in µmol/mmol creatinine, numbers refer to peak labels in Figure 1a and values in brackets are levels in unloaded controls.

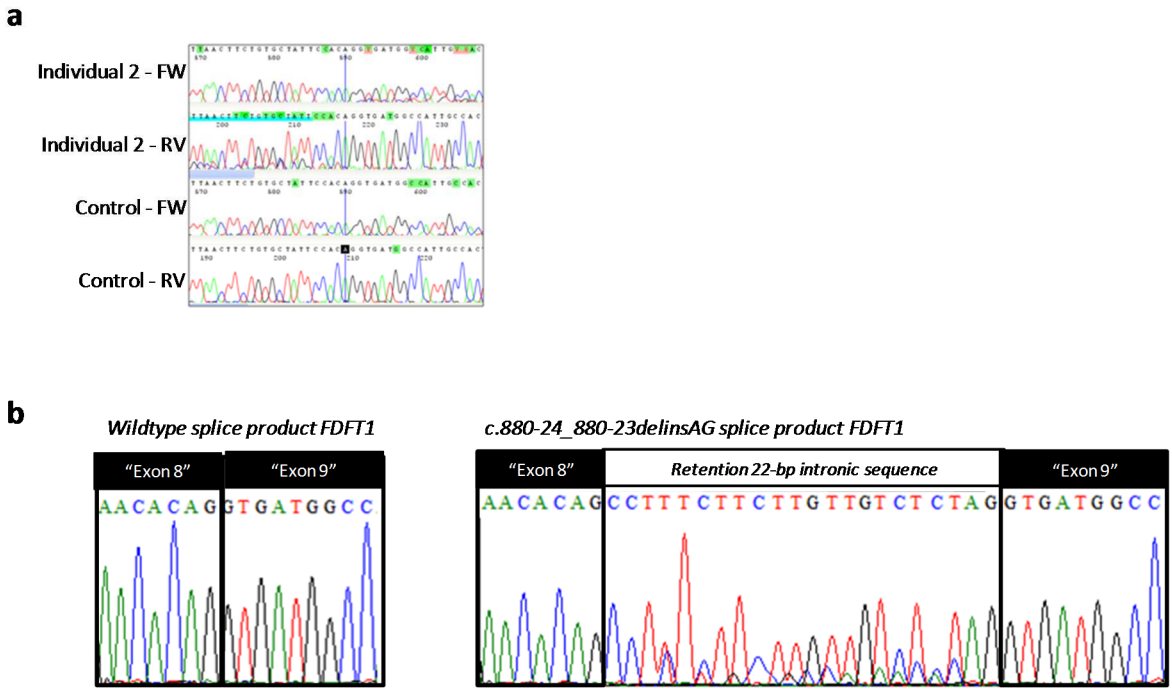

<u>Figure S2:</u> Transcriptional consequences of paternal FDFT1 splice site mutation in Individuals 1 and 2. (**a**) PCR results using *FDFT1* cDNA generated from Individual 2, with primers in exon 8 and exon 9. Top two lanes show the forward and reverse electropherograms obtained using standard Sanger sequencing. Given the deletion on the maternal allele, cDNA product is only obtained from the paternal allele. The c.880-24_880-23delinsAG variant is predicted to lead to aberrant splicing, characterized by the retention of 22 bases of intron 8 sequence. This aberrantly spliced product will result in a premature termination codon in exon 9, and is therefore expected to be degraded by nonsense mediated mRNA decay (NMD). With the wt splice acceptor still intact, it is expected that normally spliced *FDFT1* can also be detected. cDNA analysis of individual 2 indeed shows the normal splice product (from the wt acceptor splice site) as well as a lower, 2nd trace reflecting the residual aberrant splice product from incomplete NMD. (**b**) To provide further functional proof that the c.880-24_c.880-23delinsAG variant as observed in Individuals 1 and 2, results in aberrant splicing, a mini-gene splice assay was set up, using sequence of exon 8, intron 8 and exon 9. In a wildtype scenario (left), exon 8 and exon 9 are spliced together. Targeted mutagenesis to introduce the variant shows that indeed aberrant splicing occurs, as is shown by the retention of 22 bases of intron 8 sequence.

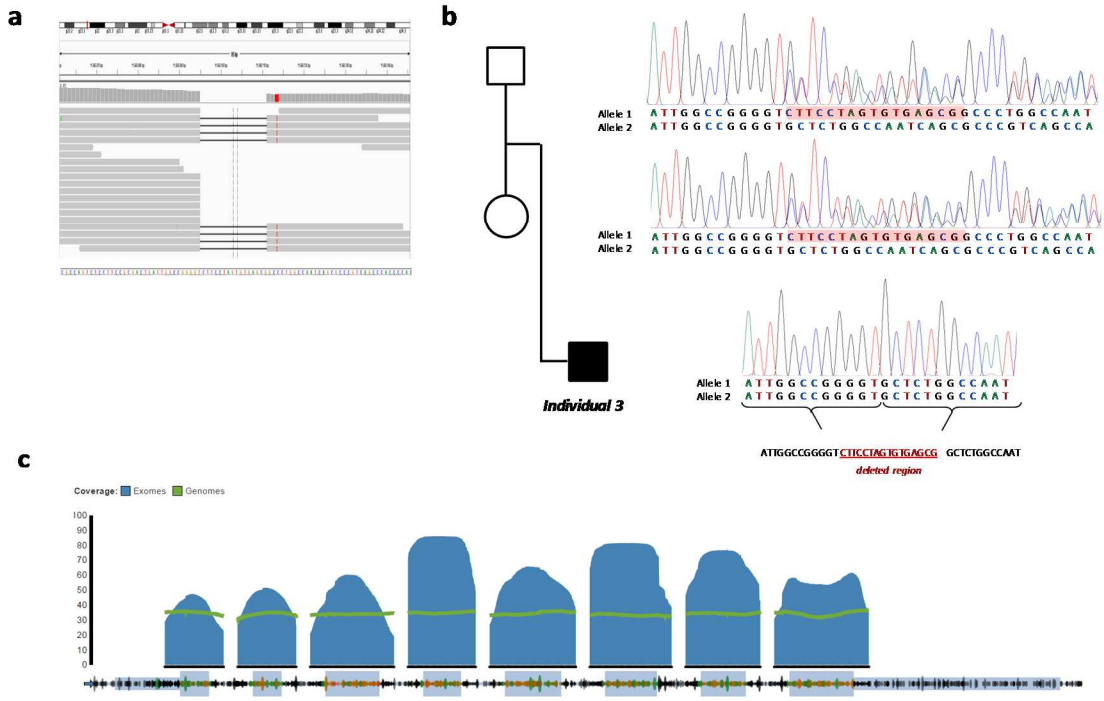

Figure S3: Screenshot of IGV displaying the BAM file from individual 3, demonstrating the coverage for this region, as well as the homozygous deletion identified in 8 reads. (**b**) Sanger validation of 16 bp deletion in Individual 3 and his parents. The deleted sequence is highlighted in red. (**c**) Screenshot from gnomAD, displaying *FDFT1* coverage information from both genomes (green) and exomes (blue), indicating overall sufficient coverage for *FDFT1* and the detection of the 16 bp deletion, if it were present in data captured in gnomAD.

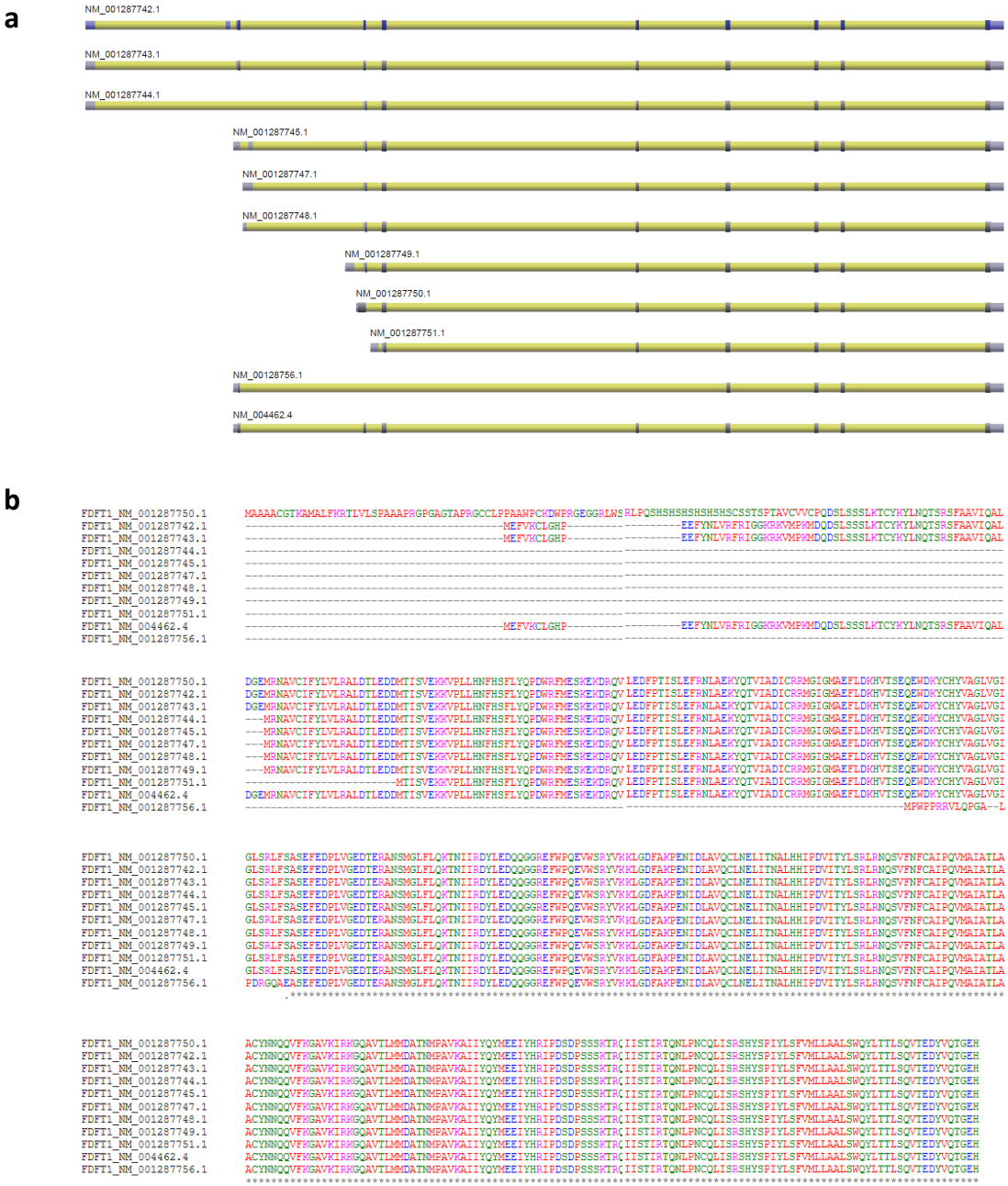

Figure S4: Schematic representation of FDFT1 and protein isoforms. (a) Overview of FDFT1 transcript isoforms based on Ref Seq. In total, 11 different transcripts for FDFT1 are reported, with the main differences being at the 5' end. Coding exons are shaded in dark grey, whereas non-coding exonic sequence is shaded in lighter grey. Intronic sequence is shown in yellow. (**b**) The 11 transcript FDFT1 isoforms result in proteins of five lengths, with the main difference being the N-terminus of the protein:

1) 476 amino acid (aa) protein is encoded by NM_01287750.1;
2) 417 aa isoform by NM_01287742.1, NM_01287743.1 and NM_04462.4;
3) 353 aa isoform by NM_01287744.1, NM_01287745.1, NM_01287747.1, NM_01287748.1 and NM_01287749.1;
4) 332 aa isoform by NM_01287750.1
5) 250 aa isoform by NM_01287756.1

a

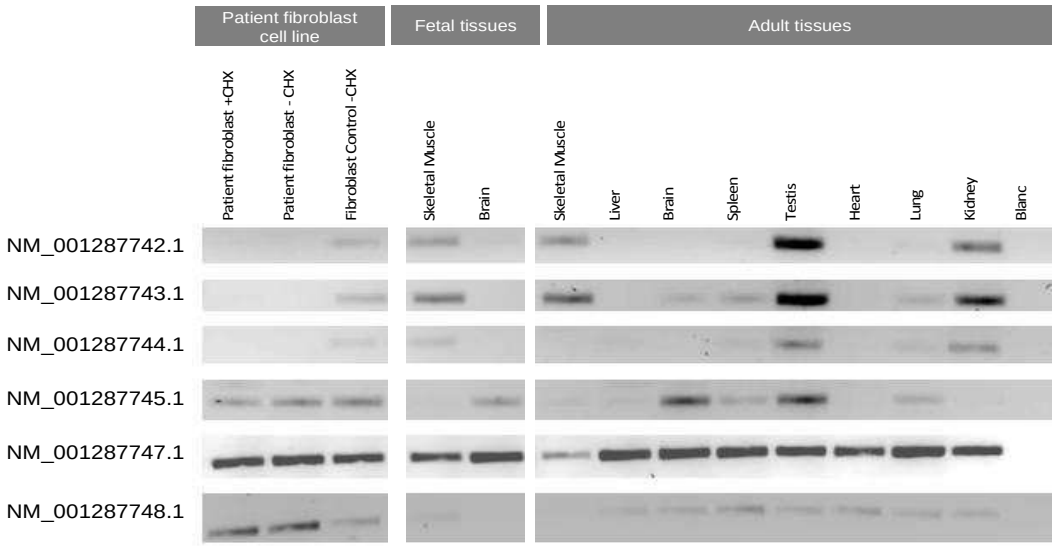

b

	Patient fibroblast			Fetal tissues		Adult tissues								
Isoform	**Patient fibroblast + CHX**	**Patient fibroblast - CHX**	**Control fibroblast – CHX**	**Skeletal muscle**	**Brain**	**Skeletal muscle**	**Liver**	**Brain**	**Spleen**	**Testis**	**Heart**	**Lung**	**Kidney**	**Blanc**
NM_001287742.1	-	-	+	+	-	+	-	-	-	+	-	-	+	-
NM_001287743.1	-	-	+	+	-	+	-	+	+	+	-	+	+	-
NM_001287744.1	-	-	+	+	-	-	-	-	-	+	-	+	+	-
NM_001287745.1	+	+	+	-	+	-	-	+	+	+	-	+	-	-
NM_001287747.1	+	+	+	+	+	+	+	+	+	+	+	+	+	-
NM_001287748.1	+	+	+	-	-	-	+	+	+	+	+	+	+	-
NM_001287749.1	+	+	+	+	+	-	+	+	+	+	+	+	+	-
NM_001287750.1	+	+	+	+	+	+	+	+	+	+	+	+	+	-
NM_001287751.1	+	+	+	+	+	+	+	+	+	+	+	+	+	-
NM_001287756.1/ NM_004462.4	+	+	+	+	+	+	+	+	+	+	+	+	+	-

<u>Figure S5:</u> FDFT1 isoforms, as well as detection of these isoforms in fibroblasts from Individual 3.(**a**) FDFT1 isoforms in fibroblasts of Individual 3 grown with cycloheximide (+CHX) and without cycloheximide (-CHX) to differentiate between absence of transcripts due to NMD or due to regulatory effects. Fibroblasts from a control individual were used to determine normal expression patterns of these isoforms in fibroblasts. Also, various organ specific cDNA libraries were tested for the normal expression patterns of these isoforms. (**b**) Simplified overview of the results presented in (a) using the following codes: +: detected; -: absent; Red: no isoform detection expected based on related control experiment; Yellow: tissues where the respective isoform is normally identified and likely absent in the patient.

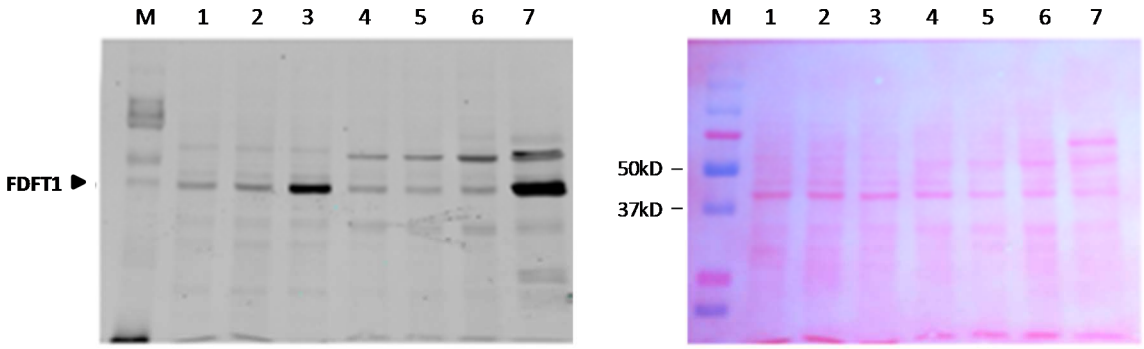

Legend:

M Marker

1. Individual 2, lymphoblasts
2. Individual 1, lymphoblasts
3. Control a, lymphoblasts
4. Individual 3, fibroblasts
5. Control b, fibroblasts
6. Control c, fibroblasts
7. Control b + FDFT1 overexpression

Figure S6: Western blot analysis Individual 3. Western blot for FDFT1 protein levels detection in Individuals 1, 2 and 3 (left). Whereas a significant FDFT1 reduction can be shown in Individuals 1 and 2 (lanes 1 and 2, compared to lane 3), no significant reduction can be identified in Individual 3 (lane 4, compared to lanes 5 and 6). Right: Ponceau S staining for loading control.

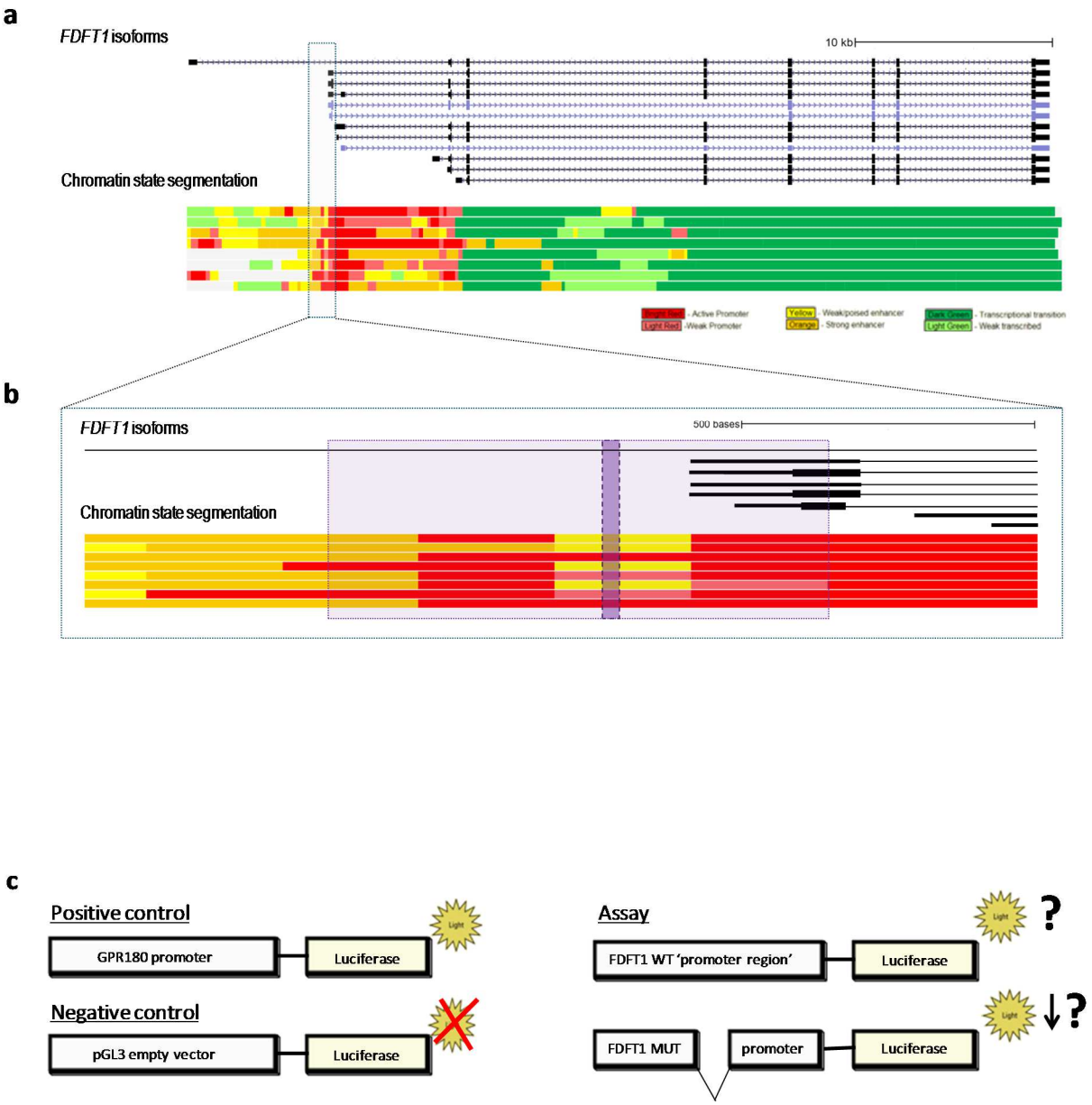

Figure S7: Schematic representation chromatin state FDFT1 isoforms and experimental set-up to assess its promoter activity.(**a**) Schematic representation of FDFT1 isoforms with annotation of chromatic state segmentation indicating that the region containing the deletion in patient 3 is predicted to have promoter (in shades of red) and/or enhancer (in shades of orange) activity based on mapping and analysis of human cell types[5,6]. (**b**) Zoom-in of the region containing the 16 bp deletion in Individual 3. The 1,024 bp-region assessed for promoter activity is highlighted in purple, with the mutation located indicated in darker purple. (**c**) Experimental set-up to test promoter activity of FDFT1. Results thereof are presented in Figure 4, and Table S1.

Supplemental Tables

Table S1: Raw and processed data of luciferase assay for assessing promoter activity of FDFT1 intronic sequence.

FDFT1 wildtype sequence								
	measurement	*Firefly Luciferase (raw data)*	*Renilla Luciferase (raw data)*	Normalization for transfection efficiency	standard deviation	Relative strength of promoter compared to empty vector	Average relative promoter strength	standard deviation
Biological replicate 1	1.1	5,253,639	18,853,700	0.28	0.01	26.11	**25.98** (100%)	**1.22** (4.68%)
	1.2	4,650,605	16,362,319	0.28		26.63		
	1.3	3,470,537	12,675,186	0.27		25.66		
Biological replicate 2	2.1	5,366,001	19,665,446	0.27	0.02	25.57		
	2.2	4,485,676	15,132,068	0.30		27.78		
	2.3	3,364,588	13,070,420	0.26		24.12		

FDFT1 mutant								
	measurement	*Firefly Luciferase (raw data)*	*Renilla Luciferase (raw data)*	Normalization for transfection efficiency	standard deviation	Relative strength of promoter compared to empty vector	Average relative promoter strength	standard deviation
Biological replicate 1	1.1	3,284,846	15,446,939	0.21	0.01	19.93	**19.78** (76%)	**0.90** (4.56%)
	1.2	4,340,171	20,590,486	0.21		19.75		
	1.3	5,530,909	24,804,902	0.22		20.89		
Biological replicate 2	2.1	3,254,900	16,763,116	0.19	0.01	18.20		
	2.2	4,440,535	21,228,426	0.21		19.60		
	2.3	5,490,335	25,354,536	0.22		20.29		

GPR180 promoter (positive control)								
	measurement	*Firefly Luciferase (raw data)*	*Renilla Luciferase (raw data)*	Normalization for transfection efficiency	standard deviation	Relative strength of promoter compared to empty vector	Average relative promoter strength	standard deviation
Biological replicate 1	1.1	320,052	9,949,642	0.03	1.66E-04	3.01	3.01	0.11
	1.2	252,404	7,858,441	0.03		3.01		
	1.3	296,761	9,151,764	0.03		3.04		
Biological replicate 2	2.1	342,483	10,659,048	0.03	1.84E-03	3.01		
	2.2	204,668	6,801,323	0.03		2.82		
	2.3	286,700	8,488,724	0.03		3.16		

pGL3 empty vector (negative control)								
	measurement	*Firefly Luciferase (raw data)*	*Renilla Luciferase (raw data)*	Normalization for transfection efficiency	standard deviation	Relative strength of promoter compared to empty vector	Average relative promoter strength	standard deviation
Biological replicate 1	1.1	328,714	30,048,130	0.01	1.13E-03	1.03	1.00	0.09
	1.2	391,524	32,767,584	0.01		1.12		
	1.3	266,326	27,482,966	0.01		0.91		
Biological replicate 2	2.1	315,404	30,272,910	0.01	1.08E-03	0.98		
	2.2	363,185	31,327,826	0.01		1.09		
	2.3	265,387	28,117,710	0.01		0.88		

None Transfected			
	measurement	*Firefly Luciferase (raw data)*	*Renilla Luciferase (raw data)*
Biological replicate 1	1.1	186	172
	1.2	135	287
	1.3	196	n.d.
Biological replicate 2	2.1	-	-
	2.2	-	-
	2.3	-	-

Supplemental Methods

Urine organic characterization GC-MS and NMR

Urine organic acids. Urine organic acid screening was performed by standard methodology involving solvent extraction, conversion to trimethylsilyl derivatives and analysis by GC-MS[1].

Plasma total farnesol and squalene measurements. Two hundred µL plasma was mixed with 200 µL of 100 mM Tris buffer pH 9.5 containing 100 mM sodium chloride and 50 mM magnesium chloride. Ten µL of alkaline phosphatase (Sigma P4439, 0.2 units/µL) was added and the mixture incubated for 15 hours at 37^{o}C. Absolute ethanol (800 µL) and 10 M sodium hydroxide (200 µL) was added and the mixture heated at 80^{o}C for 1 hour. After cooling, 1 mL of n-hexane containing paraffin mix (Supelco 4-7106 2% in n-octane, 50 µL in 50 mL of n-hexane) was added followed by vortexing and centrifuging. The upper n-hexane layer was transferred and dried under a nitrogen stream at room temperature. Pyridine (50 µL) and *N*-*tert*-butyldimethylsilyl-*N*-methyltrifluoroacetamide containing 1% *tert*-butyldimethylchloro-silane (50 µL) was added followed by incubation at 80^{o}C for 30 mins followed by addition of 150 µL of iso-octane. Samples were analysed on an Agilent 5973 GC-MS fitted with a 30 m HP-5MS column, 0.25 mm ID, 0.25 µm film. Splitless 1 µL injection were performed and the oven temperature was held at 150^{o}C for 1 min, then ramped to 320^{o}C at 10^{o}C/min and held for 2 minutes. Ions 279 (farnesol), 69 (squalene) and 71 *m/z* (C22 internal standard) were measured by selected ion monitoring. Calibrators were normal plasma spiked with free farnesol and squalene. The efficiency of alkaline phosphatase conversion of farnesyl- pyrophosphate to farnesol was checked by measuring a plasma sample spiked with farnesyl-pyrophosphate (77 and 117% recovery as farnesol).

Urine NMR. Urine of the three individuals with squalene synthase deficiency was measured with one-dimensional- and 2-dimensional COSY proton NMR spectroscopy at 500 MHz at pH 2.50 via previously described methods[2,3]

Genetic analysis

DNA isolation. Genomic DNA was extracted from whole blood using QIAamp DNA Blood Mini Kit (Qiagen, Cat# 69506), following manufacturer's specifications. Genomic DNA (gDNA) was subjected to agarose gel and OD ratio tests to confirm the purity and concentration.

Genome build. For mapping and annotation purposes referred to in this study, genome Reference Consortium Human Build 37, GRCh37, also known as hg19, was used.

Genomic microarray analysis. Genome-wide array analysis was performed by Mater Pathology Queensland using the SNP-based Cytoscan 750K array (Affymetix), with an effective resolution of 200 kb for copy number variation and 5 Mb resolution for contiguous stretches of homozygosity. Software analysis was performed using Chromosome Analysis Suite (ChAS) (Affymetrix).

Whole exome sequencing. WES was using DNA isolated from whole blood. For individuals 1 and 2, WES was performed by Otogenetics Corporation (Norcross, GA USA).) In essence, exome enrichment was based on Agilent SureSelect AV5 Exon Coverage (Agilent Technologies, Wilmington, DE USA, catalog# 5190-6208) following manufacturer's instructions, after which PE sequencing was performed with a read length of 100-106 nucleotidesat, covering 97.7% of targeted regions 100-fold and 99.7% 10-fold.

Analysis pipeline included mapping (hg19) with BWA-MEM and SAMtools, realignment and base calling with GATK Lite (2.3), variants annotation with snpEff and snpSift. The annotated

files were further analysed using Genegrid (Genomatix). Only deleterious variants with an allele frequency <0.01 according to the 1000 genomes phase 3 data set and the ExAC data set and shared by both affected siblings were considered candidates. For Individual 3 and his parents a Trio whole exome sequencing was performed commercially by Macrogen (Korea) using the Agilent SureSelect V5 capture kit, and run on an Illumina HiSeq4000 apparatus. The average read length was 101 bp and the mean depth of on-target reads was 92X. Subsequently, variants were filtered for a minor allele frequency <0.1% in ExAC and our in-house database containing 7,788 exomes, and for a strong effect on protein level (e.g. nonsense, missense, splice site and indels). Notably, after analyzing WES data of Individuals 1 and 2, pointing towards the involvement of *FDFT1*, all variants in this gene identified were searched for, including those in intronic sequences of *FDFT1* captured by WES. The latter filtering identified the private 16-bp homozygous intronic deletion. Due to its proximity to the exon, the intronic variant sequence was captured by the exome capture at a coverage over 10 reads.

Functional validation

Splice site variant analysis. Exon 9 of *FDFT1*, with flanking exon/intron boundaries, was PCR amplified from control gDNA using primers 5´-AGCAATTGCCCATTCAACAGA-3´ and 5´-ACCTGGTTAAACAGTGACATTACTA-3´. PCR product was cloned into pCR2.1-TOPO for screening and then subcloned into the pEF-1α promoter of p.EZe1.1, to create a wild-type FDFT1 clone (pEZe1.1/WT FDFT1 Ex9). The *FDFT1* c.880-24_880-23delinsAG variant was introduced using site-directed mutagenesis (QuikChange II kit, Agilent) according to the manufacturer's instructions to produce pEZe1.1/MUT FDFT1 Ex9. Clones were confirmed by Sanger sequencing. pEZe1.1/WT FDFT1 Ex9, pEZe1.1/MUT FDFT1 Ex9 and pEZe1.1 were

individually transfected into HEK293 cells using Lipofectamine 3000 (Life Technologies) according to the manufacturer's instructions. Cells were harvested 24h post-transfection and RNA extracted using an RNeasy mini kit (Qiagen). cDNA synthesis was performed on 2 µg RNA using SuperScript III reverse transcriptase (Life Technologies). Primers targeted to pEZe1.1 were used to amplify the cDNA region containing the spliced FDFT1 exon 9. Products were analysed by 1.5% (w/v) agarose gel electrophoresis and Sanger sequencing (AGRF).

To assess the effect of the c.880-24_880-23delinsAG mutation at cDNA level in individual 1 and 2, fibroblasts were grown and harvested for mRNA extraction according to standard procedures. A similar procedure was followed using control individuals. Primers designed for the full length of *FDFT1* cDNA (1441 bp) failed to produce a product, after which primers were designed to amplify part of the cDNA (993 bp). The relevant PCR products were isolated from gel and purified, after which they were sent for Sanger sequencing.

Western Blot. Immunoblotting and densitometry were performed as previously described[4], with the following modifications: membranes were probed with a 1:1000 dilution of anti-FDFT1 (Proteintech Group 13128-1-AP) or a 1:5000 dilution of anti-α-tubulin (Sigma T6199), overnight at 4°C. Control (Ctrl) and affected individuals (Ind1, Ind2Ind1, Ind2) fibroblasts were grown in media supplemented with FBS or lipid-depleted FBS (LD-FBS).

(Tissue specific) FDFT1 isoform analysis. Fibroblast cell lines of individual 3 were grown in the absence (-) and presence (+) of cycloheximide (CHX) to inhibit nonsense mediated mRNA decay. Using isoform specific PCR primers, cDNA generated from the fibroblast cell lines of individual 3 and from a control individual was tested for the presence of 10 of 11 *FDFT1* isoforms. Unique primers to distinguish NM_001287756.1 from NM_004462.4 could not be

made. In addition, organ specific cDNA libraries from fetal and adult tissues were tested for the normal patterns of these isoforms. Obtained PCR products were sequenced to verify the isoform specificity.

Luciferase assay. Gateway-tailed PCR primers (FW: GGGGACAAGTTTGTACAAAAAA GCAGGCTTCCCAAAGTGTTGCGATTACA; RV: GGGGACCACTTTGTACAAGAAAGCTGGGTGATC TTGGGCATCACCTTCC) were used to amplify a 1024 bp genomic PCR product using DNA from a control and individual 3 to assess the promoter activity under normal condition as well as when containing the 16 bp deletion respectively. The promoter sequence was subsequently introduced into entry-vector pDONR201 following the manufacturer's instructions, and transformed into DH5alpha chemically competent cells. Colonies were grown overnight at 37°C after which routine miniprep was performed for plasmid DNA isolation. The DNA insert was sequenced to exclude genetic variation other than the 16-bp deletion. Both the WT 1024 bp sequence as well as the one containing the 16 bp deletion observed in Individual 3, were cloned into pGL3 to perform the luciferase assay. pGL3 containing GPR180 and its relevant transcription were used as technical positive control, whereas an empty pGL3 basic vector was used as negative control. All constructs were co-transfected with *Renilla* to determine transfection efficiency. Luciferase activity was measured from two biological replicates (100 ng per assay) using luminometry, in triplicate. Relative promoter activity was determined by correcting for transfection efficiency, and normalization against the activity of the empty pGL3 vector.

Supplemental References

1. Pitt JJ, Peters H, Boneh A, Yaplito-Lee J, Wieser S, Hinderhofer K, Johnson D, Zschocke J. (2015). Mitochondrial 3-hydroxy-3-methylglutaryl-CoA synthase deficiency: urinary

organic acid profiles and expanded spectrum of mutations. J Inherit Metab Dis. 38:459-66.

2. Bostedor RG, Karkas JD, Arison BH, Bansal VS, Vaidya S, Germershausen JI, Kurtz MM, Bergstrom JD. (1997). Farnesol-derived dicarboxylic acids in the urine of animals treated with zaragozic acid A or with farnesol. J Biol Chem 272:9197-203.
3. Wevers, R.A. Engelke UF, Moolenaar SH, Bräutigam C, de Jong JG, Duran R, de Abreu RA, van Gennip AH. (1999). 1H-NMR spectroscopy of body fluids: inborn errors of purine and pyrimidine metabolism. Clin Chem 45:539-48.
4. Riley LG, Menezes MJ, Rudinger-Thirion J, Duff R, de Lonlay P, Rotig A, Tchan MC, Davis M, Cooper ST, Christodoulou J. (2013). Phenotypic variability and identification of novel YARS2 mutations in YARS2 mitochondrial myopathy, lactic acidosis and sideroblastic anaemia. Orphanet J Rare Dis. 8:193.
5. Ernst, J. & Kellis, M. (2010). Discovery and characterization of chromatin states for systematic annotation of the human genome. Nat Biotechnol 28:817-25.
6. Ernst J, Kheradpour P, Mikkelsen TS, Shoresh N, Ward LD, Epstein CB, Zhang X, Wang L, Issner R, Coyne M, et al., (2011). Mapping and analysis of chromatin state dynamics in nine human cell types. Nature 473(7345):43-9.